2018

Investigation on the Catalytic Performance of Reduced-Graphene-Oxide-Interpolated FeS2 and FeS for Oxygen Reduction Reaction

Hengyi Fang
University of Jinan

Taizhong Huang
University of Jinan

Jianfeng Mao
University of Wollongong, jmao@uow.edu.au

Shuo Yao
University of Jinan

M Dinesh
University of Jinan

See next page for additional authors

Publication Details

Fang, H., Huang, T., Mao, J., Yao, S., Dinesh, M. Mayilvel., Sun, Y., Liang, D., Qi, L., Yu, J. & Jiang, Z. (2018). Investigation on the Catalytic Performance of Reduced-Graphene-Oxide-Interpolated FeS2 and FeS for Oxygen Reduction Reaction. ChemistrySelect, 3 (37), 10418-10427.

Investigation on the Catalytic Performance of Reduced-Graphene-Oxide-Interpolated FeS2 and FeS for Oxygen Reduction Reaction

Abstract
The oxygen reduction reaction (ORR) plays a key role in many kinds of energy conversion and energy storage devices, especially in fuel cells. Developing low-cost, easily prepared, and high-efficiency catalysts is a crucial factor for the large-scale applications of fuel cells. Herein, we report the reduced graphene oxide (rGO) interpolated FeS2and FeS as low cost and high performance electrocatalyst for ORR in the alkaline electrolyte. Cyclic voltammetry tests indicate that the onset potential of the ORR for FeS2@rGO is −0.142 V, which is close to the state-of-the-art commercial Pt/C (-0.114 V) catalyst. A low Tafel slope of ~ 98 mV/decade and high durability are also observed for the FeS2@rGO composite for ORR. The reaction kinetics study shows that the rGO-interpolated FeS2catalyzed ORR major happen through 4-electron pathway, but the rGO-interpolated FeS catalyzed ORR major happen through mixed 2-electron and 4-electron pathway. The S−S bond of FeS2play the major role for the happening of ORR through 4-electron pathway.

Keywords
reduction, oxygen, fes, fes2, reduced-graphene-oxide-interpolated, catalytic, performance, investigation, reaction

Disciplines
Engineering | Physical Sciences and Mathematics

Publication Details
Fang, H., Huang, T., Mao, J., Yao, S., Dinesh, M. Mayilvel., Sun, Y., Liang, D., Qi, L., Yu, J. & Jiang, Z. (2018). Investigation on the Catalytic Performance of Reduced-Graphene-Oxide-Interpolated FeS2 and FeS for Oxygen Reduction Reaction. ChemistrySelect, 3 (37), 10418-10427.

Authors
Hengyi Fang, Taizhong Huang, Jianfeng Mao, Shuo Yao, M Dinesh, Yue Sun, Dong Liang, Lei Qi, Jiemei Yu, and Zhankun Jiang

Investigation on the Catalytic Performance of Reduced Graphene Oxide Interpolated FeS_2 and FeS for Oxygen Reduction Reaction

Hengyi Fang, [a] Taizhong Huang,* [a] Jianfeng Mao,*[b] Shuo Yao, [a] M. Mayilvel Dinesh, [a] Yue Sun, [a] Dong Liang, [a] Lei Qi, [a] Jiemei Yu, [a] and Zhankun Jiang[a]

Abstract: The oxygen reduction reaction (ORR) plays a key role in many kinds of energy conversion and energy storage devices, especially in fuel cells. Developing low-cost, easily prepared, and high-efficiency catalysts is a crucial factor for the large-scale applications of fuel cells. Herein, we report the reduced graphene oxide (rGO) interpolated FeS_2 and FeS as low cost and high performance electrocatalyst for ORR in the alkaline electrolyte. Cyclic voltammetry tests indicate that the onset potential of the ORR for FeS_2@rGO is -0.142 V, which is close to the state-of-the-art commercial Pt/C (-0.114 V) catalyst. A low Tafel slope of ~ 98 mV/decade and high durability are also observed for the FeS_2@rGO composite for ORR. The reaction kinetics study shows that the rGO-interpolated FeS_2 catalyzed ORR major happen through 4-electron pathway, but the rGO-interpolated FeS catalyzed ORR major happen through mixed 2-electron and 4-electron pathway. The S-S bond of FeS_2 play the major role for the happening of ORR through 4-electron pathway.

1. Introduction

Owing to the increasing energy crisis and environmental pollution that resulted from the heavy consumption of fossil fuels, clean energy resources such as wind and solar are playing more and more important roles in the energy field.[1] In order to adopt these intermittent renewable energies efficiently, technologies have been developed to meet the demands of energy conversion and storage.[2] Hence, there is significant interest in electrochemical energy conversion and storage technologies such as fuel cells, batteries, and supercapacitors. Among these devices, fuel cells are of particular interest due to their benefits of high energy intensity, rapid start-up, zero emissions, environmental friendliness, low operating temperature, etc.[3] In general, fuel cell devices generate electricity through electrochemical energy conversion between the anode (hydrogen, methanol, ethanol, etc.) and the cathode (air/oxygen from the atmosphere), where the ions move between the anode and cathode through the electrolyte; whereas the electrons liberated from the anode reach the cathode through the external circuit.[4] A major limiting factor for the energy-conversion efficiency of fuel cells is the sluggish reaction kinetics of the oxygen reduction reaction (ORR) at the cathode, which is determined by the performance of the catalysts on the electrode.[5]

[a] Hengyi Fang, Prof. Taizhong Huang, Shuo Yao, Dr. M. Mayilvel Dinesh, Yue Sun, Dong Liang, Dr. Lei Qi, Dr. Jiemei Yu, and Dr. Zhankun Jiang
Shandong Provincial Key Laboratory of Fluorine Chemistry and Chemical Materials, School of Chemistry and Chemical Engineering
University of Jinan
Jinan 250022, P.R. China
E-mail: chm_huangtz@ujn.edu.cn
[b] Dr. Jianfeng Mao
Institute for Superconducting & Electronic

Although the platinum (Pt) based catalysts are the most popular ORR catalysts at present, the shortcomings of high cost, easily poisoned, and sluggish activity have become obstacles on the large-scale applications of fuel cells.[6] Therefore, developing high-performance and low-cost electrocatalysts for ORR is the key factor for promoting the wide applications of fuel cells.[7]

Recent studies have shown that the integration of electrocatalyst with conducting support such as carbon nanomaterials, is an effective way to developing catalysts with both high catalytic performance and long-time running stability. [8] The combination of the transition metal-based catalyst with conductive nanocarbons represents a promising strategy to improve the overall catalytic performance towards ORR.[9] Compared to the traditional carbon-based materials (carbon nanotubes, carbon black), graphene has special catalytic characteristics for the ORR.[10] Firstly, the graphene, as support for the catalyst, has a strong affinity with other catalysts. Secondly, the graphene also shows some extent catalytic performance towards ORR, which could make it more effective in the catalytic process.[11] The peak current intensity of some graphene-interpolated transition metal based catalysts for ORR even surpass that of commercial Pt/C catalyst.[12] Kinds of transition metal-based catalysts for ORR such as metal oxides, carbides, nitrides, and chalcogenides have been reported.[13] The favorable performance can be attributed to the incomplete outermost *d* orbital electrons of the transition metal atoms. Among the transition metal elements, the first-row transition metal chalcogenides (e.g. V, Ti, Fe) have emerged as high promising catalysts for ORR owning to their advantages of abundant sources, low cost, and considerable activity.[14] The catalytic performance of transition metal based catalysts for ORR can be improved by constructing novel structure and high catalytic active sites, which enhance the efficiency of mass transfer. The catalytic performance of metal sulfides has been reported. But the difficulty of the synthesis of transition metal sulfides with high purity has inhibited their applications as catalysts for ORR.[15, 16]

In this work, we synthesized FeS_2, FeS, and their nanocomposites with interpolated reduced graphene oxide (rGO), that is, FeS_2@rGO and FeS@rGO, with high purity, and investigated their catalytic performances for ORR in alkaline electrolyte. It was found that the rGO interpolated FeS_2 and FeS exhibit superior catalytic activity for ORR. Among all the catalysts, FeS_2@rGO shows the highest catalytic performance for ORR. To the best of our knowledge, there are scarce report on the rGO interpolated FeS_2 as catalyst for ORR in alkaline electrolyte. FeS_2@rGO shows better stability than the benchmark Pt/C catalysts for ORR. FeS_2@rGO has great

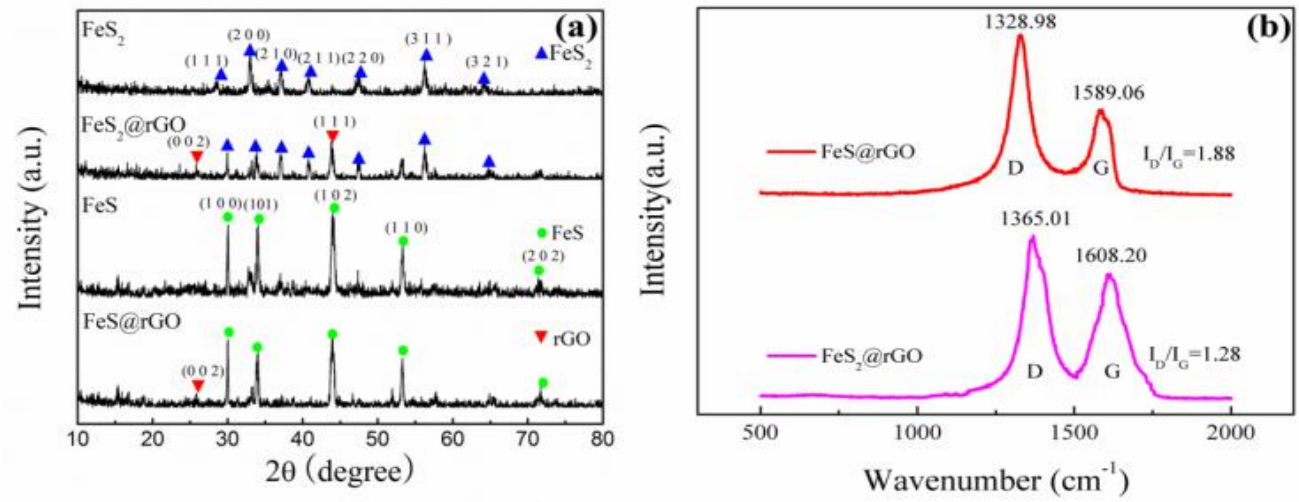

Figure 1. (a) XRD patterns of FeS, FeS@rGO, FeS_2, and FeS_2@rGO. (b) Raman spectra of FeS@rGO and FeS_2@rGO.

potential to be high performance catalyst for the ORR in cathodes of alkaline fuel cells.

Results and Discussion

Structural Properties of FeS, FeS@rGO, FeS_2, and FeS_2@rGO

The synthesis procedure of FeS, FeS@rGO, FeS_2 and FeS_2@rGO are illustrated in Figure S1. The XRD patterns of the synthesized FeS, FeS@rGO, FeS_2, and FeS_2@rGO are shown in Figure 1a. FeS was easily indexed in both FeS and FeS@rGO, and the corresponding Joint Committee on Powder Diffraction Standards (JCPDS) file number is 65-9124. The indexed results indicate that the FeS has a primitive hexagonal structure. The calculated cell parameters *a* and *c* of FeS are 0.345 and 0.569 nm, respectively. Similarly, FeS_2 is indexed in both FeS_2 and FeS_2@rGO, and the corresponding JCPDS file number is 65-3321, which indicates that the FeS_2 has a face-centered cubic (FCC) structure. The calculated cell parameter *a* of FeS_2 is 0.542 nm. The diffraction peak around 27.2°, which is obtained both in FeS_2@rGO and FeS@rGO, could be attributed to the rGO (002) planes.[17]

The presence of rGO in FeS@rGO and FeS_2@rGO was further confirmed by Raman spectroscopy, as shown in Figure 1b. The typical D and G peaks are clearly found in the Raman spectra of both FeS@rGO and FeS_2@rGO, which prove the presence of rGO. Interestingly, the obtained D and G peaks of FeS@rGO are centered at 1328.98 cm^{-1} and 1589.06 cm^{-1}, respectively, but for FeS_2@rGO, the obtained D and G peaks are centered at 1365.01 cm^{-1} and 1608.20 cm^{-1}. The changes of the corresponding wavenumbers of the D and G peaks between FeS@rGO and FeS_2@rGO should be induced by the FeS and FeS_2. The intensity ratios of D to G peaks, I_D/I_G, of FeS@rGO and FeS_2@rGO are 1.88 and 1.28, respectively, which means that there are fewer defects in the rGO of FeS_2@rGO than that of FeS@rGO.[18] The low I_D/I_G of FeS_2@rGO should be attributed to the annealing treatment, which inhibits the occurrence of structural defects.[19]

XPS measurements were carried out to examine the elemental compositions and atomic bonding states of FeS, FeS_2, and their interaction with rGO. The full spectra of FeS, FeS_2, FeS@rGO, and FeS_2@rGO distinctly reveal the presence of Fe and S in the desired stoichiometric ratio (Figures S2-S5). The high-resolution XPS of Fe and S of FeS@rGO and FeS_2@rGO have been deconvoluted, and the results are shown in Figure 2a and 2c. Figure 2a shows that the Fe $2p_{3/2}$ and Fe $2p_{1/2}$ peaks of Fe of FeS_2@rGO at 709.5 and 722.8 eV, respectively. Figure 2b shows that the XPS of S 2p of Fe of FeS@rGO.The two peaks with centered at 161.3 and 162.5 eV should be assigned to S $2p_{3/2}$ and S $2p_{1/2}$, respectively. For FeS_2@rGO (Figure 2c), the binding energies for Fe $2p_{3/2}$ and Fe $2p_{1/2}$ are centered at 708.6 and 721.3 eV, respectively. The binding energies of Fe 2p of FeS@rGO and FeS_2@rGO only show small differences. The binding energy of Fe 2p peaks of FeS@rGO and FeS_2@rGO shifted to higher binding energy direction compared to the pristine FeS or FeS_2, which should be attributed to the migration of metal electrons that induced by the strong electronegativity of O species on the rGO surface. The intimate interaction between rGO and metal sulfides renders the catalysts high conductivity and electrochemical activity. Figure 2d shows the XPS of S 2p of FeS_2@rGO. The two strong peaks at 163.9 and 165.1 eV are corresponding to the S $2p_{3/2}$ and S $2p_{1/2}$ peaks, respectively. Comparison of the S 2p peaks of FeS and FeS_2 shows that the binding energy of S-Fe bond of FeS_2 is stronger than that of FeS, which is the most obvious feature to distinguish these two catalysts.[20] The two small peaks corresponding to the binding energy of 170.0 and 171.3 eV of Figure 2d should be attributed to -C-SO_x-C bonds.[21] The XPS test results demonstrate the successful synthesis of FeS, FeS_2, FeS@rGO and FeS_2@rGO.

Typical SEM images and low resolution TEM images of FeS@rGO and FeS_2@rGO are shown in Figure 3. The SEM

images of FeS@rGO show regular hexagonal sheets (FeS) which are enveloped by the rGO (Figure 3a).[22]

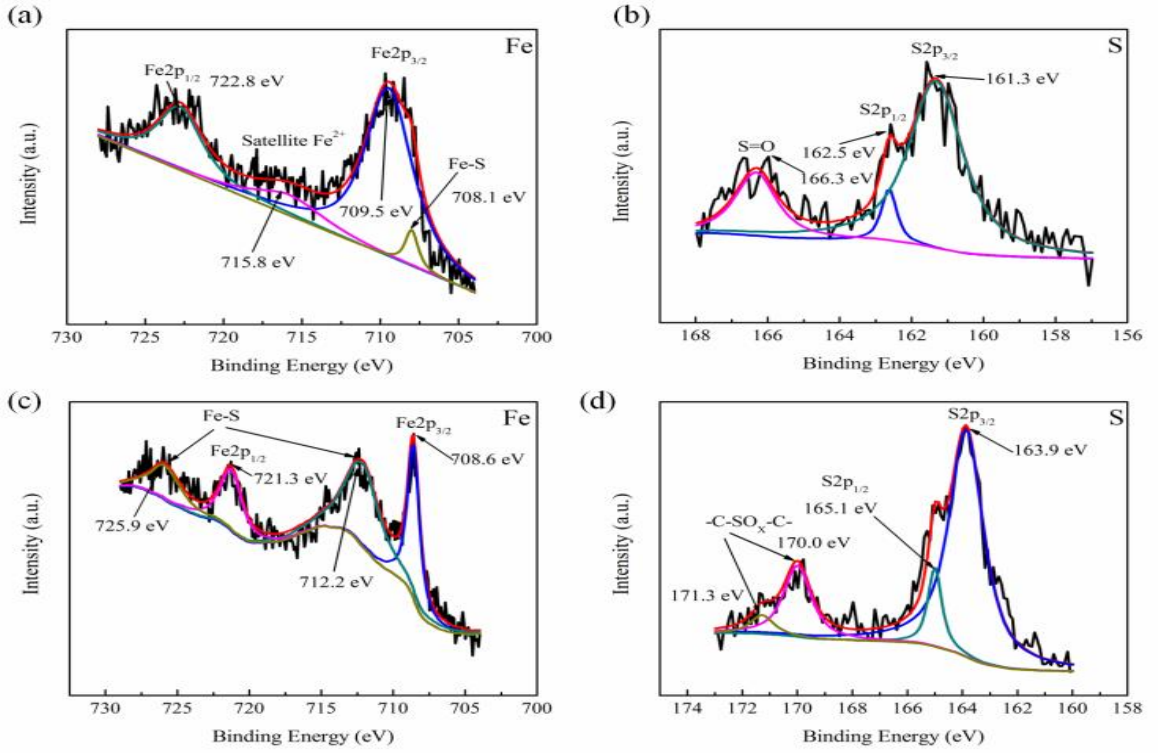

Figure 2. High-resolution XPS of Fe in FeS@rGO (a) and FeS_2@rGO (c); High-resolution XPS of S in FeS@rGO (b) and FeS_2@rGO (d).

The hexagonal shape of FeS is consistent with the SEM test results (Figure S6a, Supporting Information). Compared with the sheet-like FeS, FeS_2@rGO in Figure 3b and pristine FeS_2 in Figure S6b show an octahedral structure.

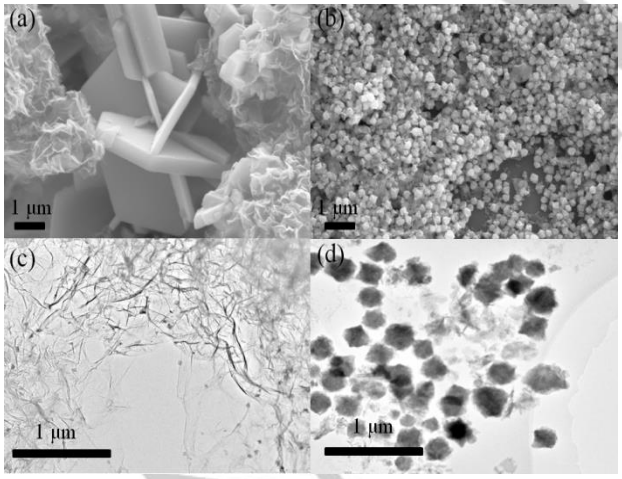

Figure 3. SEM images of FeS@rGO nanosheets (a) and FeS_2@rGO nanoparticles (b), low- resolution TEM images of FeS@rGO (c) and FeS_2@rGO (d).

The TEM image in Figure 3c shows that the FeS nanosheets are evenly distributed on the rGO sheets, which is consistent with the SEM image (Figure 3a). Figure 3d shows that the FeS_2 particles are also distributed on the rGO sheets. Compared with the pristine FeS_2 (Figure S6d), the size distributions of FeS_2 in FeS_2@rGO is more uniform. Based on the SEM results, the obtained element mappings of FeS, FeS@rGO, FeS_2, and FeS_2@rGO are shown in Figures S7-S10 (Supporting Information). The elemental mapping of each catalyst shows the signal of compositional elements. And the distributions of all the elements are consistent with each other, which prove the successful synthesis of each catalyst.

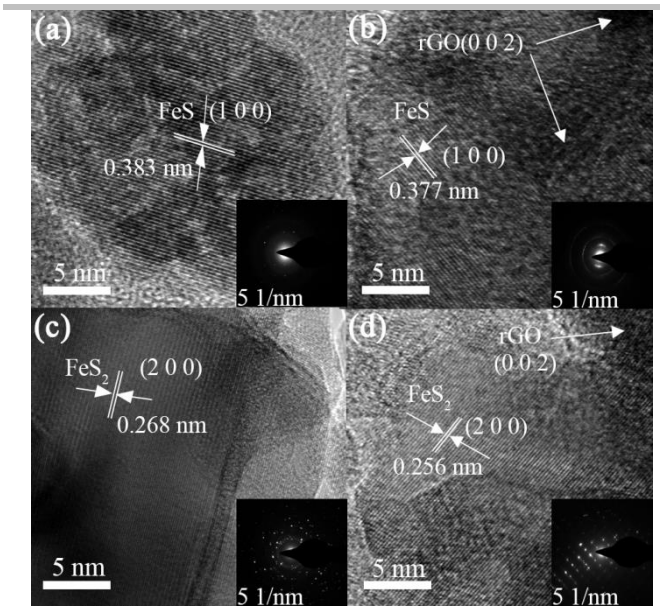

Figure 4. HRTEM images of FeS (a), FeS@rGO(b), FeS_2 (c), and FeS_2@rGO (d). The insets in (a), (b), (c), and (d) are the corresponding SAED patterns.

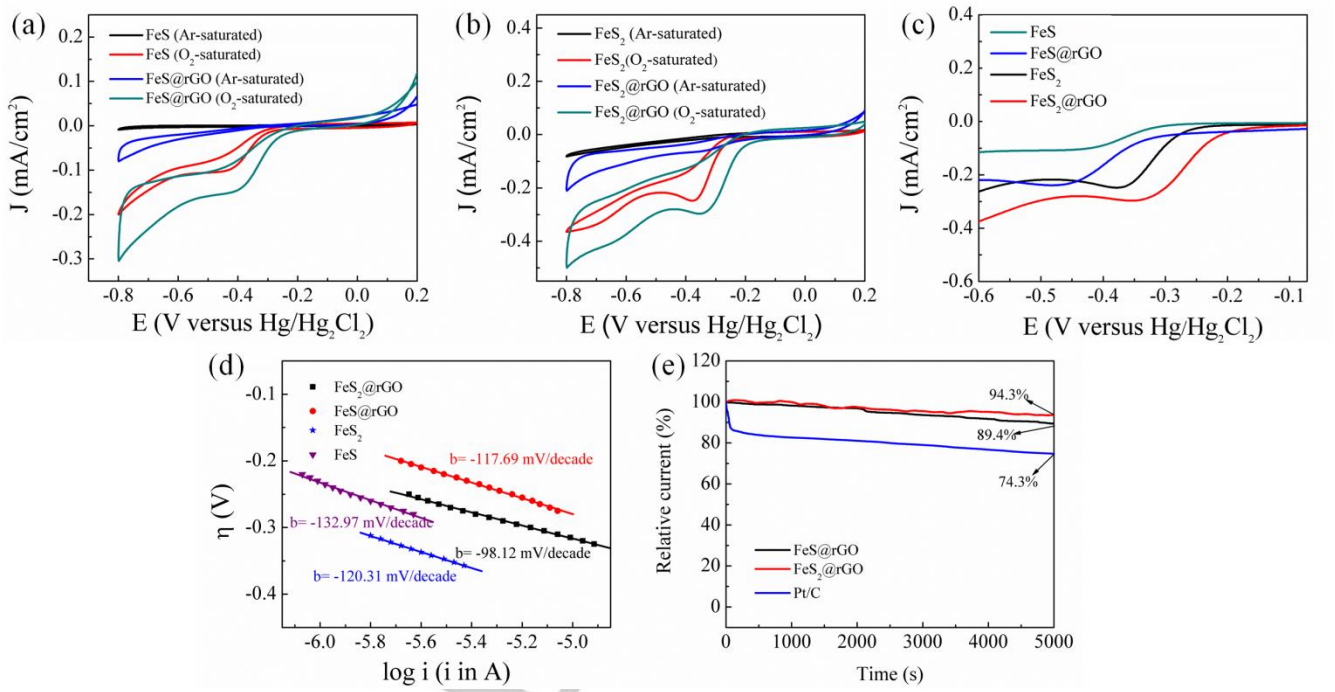

Figure 5. CV tests of FeS and FeS@rGO (a), FeS_2 and FeS_2@rGO (b) in both oxygen and argon saturated electrolyte, respectively; LSV tests (c) and Tafel (d) tests of FeS, FeS@rGO, FeS_2 and FeS_2@rGO; (e) The chronoamperometric tests of FeS@rGO, FeS_2@rGO, and Pt/C catalysts.

The HRTEM image of FeS in Figure 4a clearly shows that the crystal lattice spacing is 0.383 nm, which is corresponding to the (100) facet of FeS. Figure 4b shows the HRTEM image of FeS@rGO. (100) facet of FeS with the lattice spacing of 0.377 nm is also detected. On the other hand, the (002) facet of rGO is also detected in Figure 4b, which illustrates the successful synthesis of FeS@rGO. The SAED patterns of FeS and FeS@rGO are quite similar, which proves the presence of FeS in both of them. Figure 4c and 4d show the HRTEM images of FeS_2 and FeS_2@rGO, respectively. The (200) facet of FeS_2 are detected in both of them. On the other hand, the SAED patterns of both catalysts are also quite similar, which also proves the successful synthesis of FeS_2 in both of them. Based on the HRTEM and SAED results, the well-ordered and assembled structure can be attributed to the intrinsic crystal characteristics of the coordination interaction.[23]

The catalytic performances of the catalysts for ORR are firstly examined by CV tests and the results are showed in Figure 5a and 5b.

Figure 5a and 5b show the CV tests of FeS and FeS@rGO, and FeS_2 and FeS_2@rGO in oxygen and argon saturated 0.1 M KOH electrolyte with the sweeping rate of 0.005 V s^{-1}, respectively. It can be seen that, for all the catalysts, no

peaks could be detected in the argon saturated electrolyte, which means that all the catalysts can remain stable in the electrolyte during the test process. In contrast, obvious peaks are distinctly detected in the CV curves of the oxygen saturated electrolyte, which means that the oxygen could be reduced by all the catalysts. Based on the CV tests, the onset potential (E_{onset}), peak current potential (E_p) and peak current intensity (J_p) of the oxygen reduction reaction are obtained, and the results are shown in Table 1.

Table 1 The E_{onset}, E_p, and J_p of FeS, FeS@rGO, FeS_2, FeS_2@rGO, and Pt/C catalysts

Catalyst	E_{onset} (V)	E_p (V)	J_p (mA cm^{-2})
FeS	-0.284	-0.455	0.103
FeS@rGO	-0.249	-0.406	0.146
FeS_2	-0.208	-0.351	0.251
FeS_2@rGO	-0.142	-0.316	0.332
Pt/C	-0.114	-0.269	0.440

It is clearly observed that, compared with other catalysts, the onset potential and peak current potential of FeS_2@rGO exhibit a huge shift to the positive direction compared with other catalysts. On the other hand, the FeS_2@rGO catalyzed ORR also shows the highest peak current intensity in all the catalysts. The onset potential of FeS_2@rGO is -0.142 V, which is just 0.028 V lower than that of the Pt/C catalyst.[24] The FeS_2@rGO shows the highest catalytic activity for ORR, which is further confirmed by the LSV tests (Figure 5c).

Figure 5c shows the LSV tests of FeS, FeS@rGO, FeS_2, and FeS_2@rGO. It is clearly observed that the results are consistent with the CV test results. Compared with the pristine FeS or FeS_2, the rGO interpolated catalysts exhibit higher onset potential and higher peak current intensity, which should be attributed to the enhanced conductivity and synergistic effect of rGO.[25] In particular, the catalytic performance for the ORR of FeS_2@rGO hybrid is close to that of super Pt/C catalyst in terms of the onset potential and the peak current intensity.[26]

The superior ORR catalytic activity of FeS_2@rGO is also confirmed by its low Tafel slope as shown in Figure 5d. The Tafel slopes of FeS, FeS@rGO, FeS_2, and FeS_2@rGO are 132.97, 117.69, 120.31 and 98.12 mV·$decade^{-1}$, respectively. The Tafel slope of FeS_2@rGO is even lower than that of Pt/C catalyst (119 mV·$decade^{-1}$).[27] FeS_2@rGO has the lowest polarization potential among the four catalysts, which is benefit to the continuous long-time running stability. Based on the Tafel tests, the exchange current intensity and electron transfer coefficient of ORR with the catalysts could be calculated according to Tafel's equation (1):[28]

$$\eta = a + b\,log\,i = -\frac{2.303\,RT}{\alpha nF}log\,i_0 + \frac{2.303\,RT}{\alpha nF}log\,i \qquad (1)$$

Where η is the overpotential, a is the intercept of the Tafel plot, b is the Tafel slope, R is the universal gas constant (8.314 J/(mol·K)), T is the temperature in K, F is the Faraday constant 96485 C/mol, n is the reaction electron number, α is the electron transfer coefficient, and i_0 is the exchange current intensity on the catalyst surface. The calculated α and i_0 are shown in Table 2. Clearly, the FeS_2@rGO shows the highst electron transfer coefficient and exchange current intensity, which also confirms that the electrocatalytic activity of FeS_2@rGO is the highest among the four catalysts.

The long-time running stability of the catalysts is investigated by the current-time chronoamperometric tests, and the results are shown in Figure 5e. The results show that, apart from high catalytic activity, the FeS_2@rGO catalyst also exhibits the highest catalytic durability. After a continuous 5000 s running, the current intensity of FeS_2@rGO is still remained above 94.3%, which is significantly higher than that of the benchmark Pt/C (74.3%), and the FeS@rGO (89.4%). As comparison, the current-time chronoamperometric test results for FeS and FeS_2 are shown in Figure S11, which also demonstrates that the relative current intensity can be kept at 92.4% and 94.4%. The differences in the long-term running stability of these four catalysts should be attributed to their intrinsic structure characteristics and the influence of the interpolated rGO.

The electrocatalytic activity and electron kinetics for ORR of the FeS@rGO and FeS_2@rGO catalysts were also investigated by using rotating disk electrode (RDE) tests. The RDE tests of FeS@rGO and FeS_2@rGO are shown in Figure 6, respectively, while the RDE tests for FeS andFeS_2 are supplied in Figure S12. It is distinctly observed that, to each catalyst, the current intensity of ORR increases with the increase of rotating speed at the same potential, which should be attributed to the enhanced oxygen diffusion on the electrode.[29] It can also be seen from the results that the current intensity of FeS@rGO and FeS_2@rGO are higher than of pristine FeS and FeS_2.

Table 2 Tafel slope, electron transfer coefficient and exchange current intensity of the FeS, FeS@rGO, FeS_2, and FeS_2@rGO for ORR.

Catalyst	b (mV dec^{-1})	α	i_0 (mA cm^{-2})
FeS	132.97	0.21	1.8×10^{-8}
FeS@rGO	117.69	0.28	3×10^{-8}
FeS_2	120.31	0.24	4.1×10^{-8}
FeS_2@rGO	98.12	0.34	6.2×10^{-8}

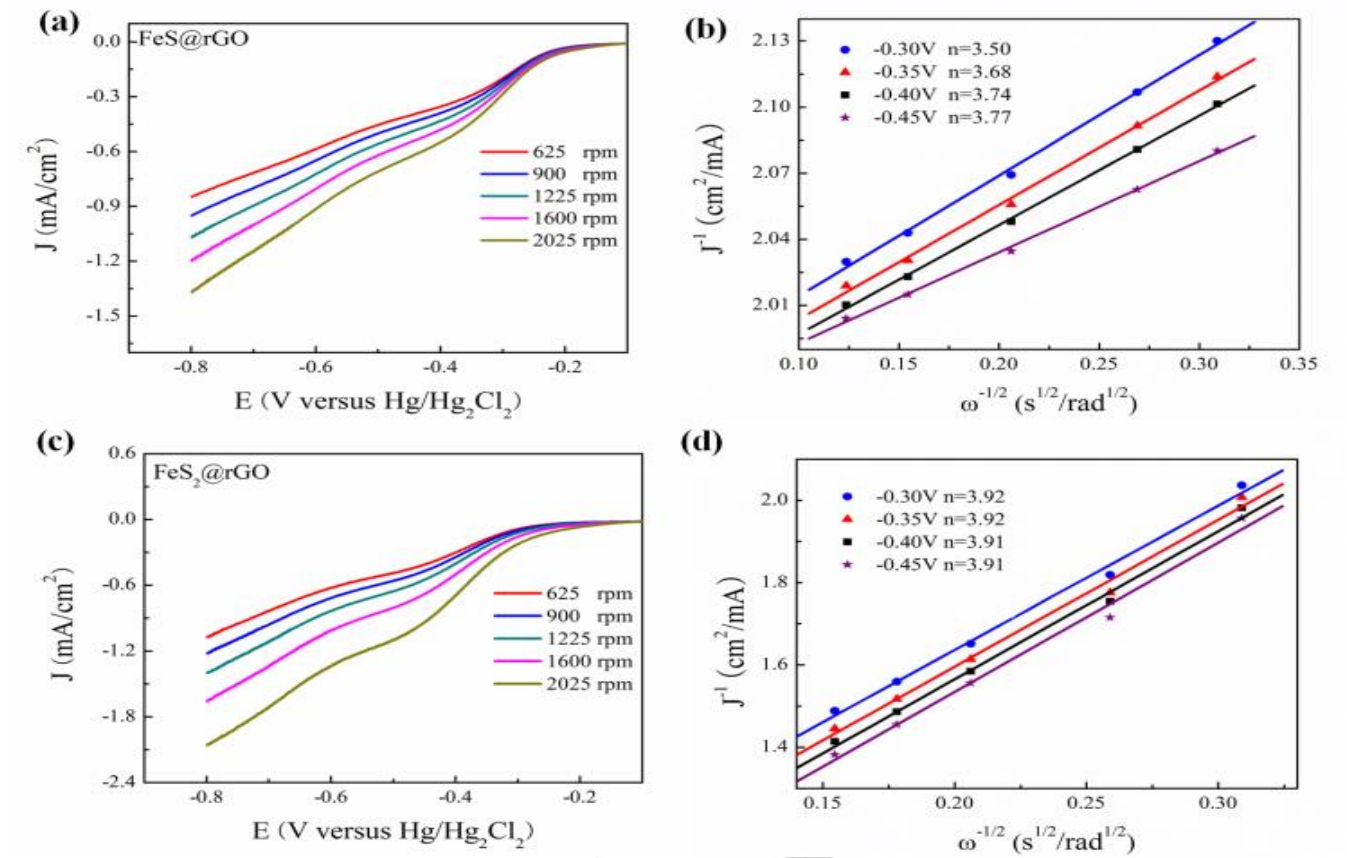

Figure 6. RDE tests and corresponding K–L lines of FeS@rGO (a) and (b), and FeS_2@rGO (c) and (d) in oxygen saturated 0.1 M KOH at different rotating speeds with the sweeping rate of 0.005 V s^{-1}.

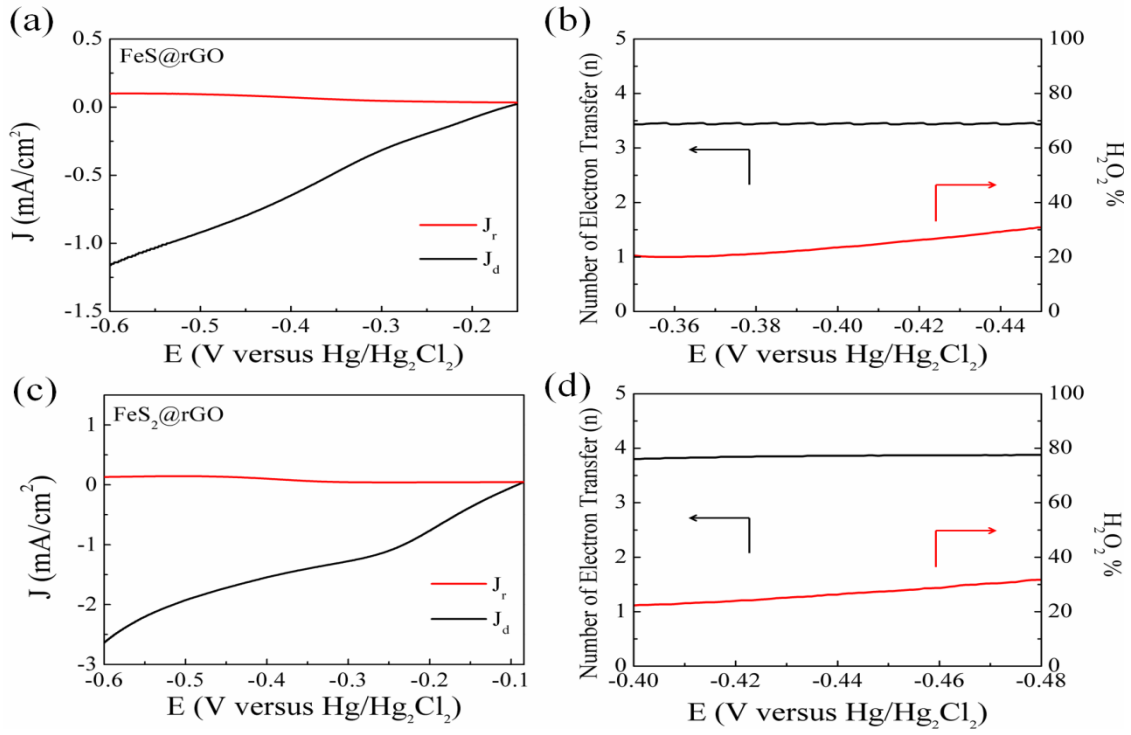

Figure 7. RRDE test results of (a) FeS@rGO and (c) FeS_2@rGO at 1600 rpm, and the corresponding electron transfer numbers (*n*) and the percentage of H_2O_2 % of FeS@rGO (b) and FeS_2@rGO (d).

Based on the RDE tests, the electron transfer number (*n*) can be calculated according to the Koutechy-Levich (K-L) equation (2):[30]

$$\frac{1}{J} = \frac{1}{J_L} + \frac{1}{J_K} = \frac{1}{B\omega^{-1/2}} + \frac{1}{J_K} \quad (2)$$

where *J* is the measured current intensity, J_K is the kinetic current intensity, J_L is the diffusion limiting current intensity, and *ω* is the electrode rotating speed. *B* is the slope of the K-L line, as defined in the Koutechy-Levich equation, which can be written as Equation (3):[31]

$$B = 0.62nFC_0(D_0)^{2/3}\upsilon^{-1/6} \quad (3)$$

where *n* is the electron transfer number, *F* is the Faraday constant: 96,485 C mol^{-1}, D_0 (1.9×10^{-5} cm^2 S^{-1}) is the diffusion coefficient of O_2 in the 0.1 M KOH electrolyte, *υ* (0.01 cm^2 s^{-1}) is the kinetic viscosity, and C_0 (1.2×10^{-6} mol cm^{-3}) is the bulk concentration of O_2 in the electrolyte. The constant 0.62 is adopted when the rotating speed *ω* is expressed in rad/s. The electron transfer numbers are calculated from the slopes of the K-L plots, and the results are shown in Figure 6 (FeS@rGO and FeS_2@rGO) and Figure S12 (FeS and FeS_2). The obtained electron transfer numbers of FeS, FeS@rGO, FeS_2, and FeS_2@rGO are 3.41, 3.67, 3.69 and 3.92, respectively. Based on the results, it can be deduced that the ORR mainly happen through 4-electron pathway. Only a small amount of oxygen is reduced through 2-electron pathway. The 4-electron and 2-electron ORR pathways are as follows:[32]

4-electron pathway: $O_2 + 2H_2O + 4e^- \rightarrow 4OH^-$ (4)

2-electron pathway: $O_2 + 2H_2O + 2e^- \rightarrow 2OH^- + H_2O_2$ (5)

$$H_2O_2 + 2e^- \rightarrow 2OH^- \quad (6)$$

Similarly, the calculated electron transfer number (*n*) and the percentage of generated hydrogen peroxide were further evaluated by using rotating ring disk electrode (RRDE) tests. Figure 7 shows the current intensity of disc electrode and collection ring of Pt. Based on the RRDE tests, the electron transfer number and the percentage of H_2O_2 were calculated according to the Eqs. (7) and (8):[33]

$$n = \frac{4\times I_d}{I_d + I_r/N} \quad (7)$$

$$H_2O_2 = 200 \times \frac{I_r/N}{I_d + I_r/N} \quad (8)$$

where I_d is the disk current, I_r is the ring current, and *N* is the geometrical current collection coefficient of Pt in the RRDE (0.39). Figure 7c clearly shows that the current intensity of FeS_2@rGO and FeS@rGO is 2.7 mA cm^{-2} and 1.1 mA cm^{-2}, respectively. As shown in Figure 7 and Figure S13, the calculated electron transfer number for FeS, FeS@rGO, FeS_2, and FeS_2@rGO are 3.48, 3.85, 3.72 and 3.92, respectively. The results are consistent with the RDE test results. The obtained percentages of H_2O_2 are 32.5%, 24.8%, 33.4% and 15.8%, respectively. Based on the RDE and RRDE tests, it could be deduced that the 4-electron and 2-electron pathways of the ORR coexisted on the electrode. The occurrence of the 2-electron reaction is also inevitable in theory.[34] The outer-sphere electron transfer mechanism in alkaline media is likely to be responsible for the unwanted 2-electron hydrogen peroxide intermediate.[35] The inner-sphere electrocatalytic process is the direct cause of the 4-electron pathway.

A Faradaic Efficiency determination and post catalysis XPS analysis were test, which in order to exploring the stability of all the catalysts in the O_2-saturated 0.1M KOH electrolyte. In addition, the RRDE was tested at a ring potential at -0.4 V to gain insight into the reaction mechanism.

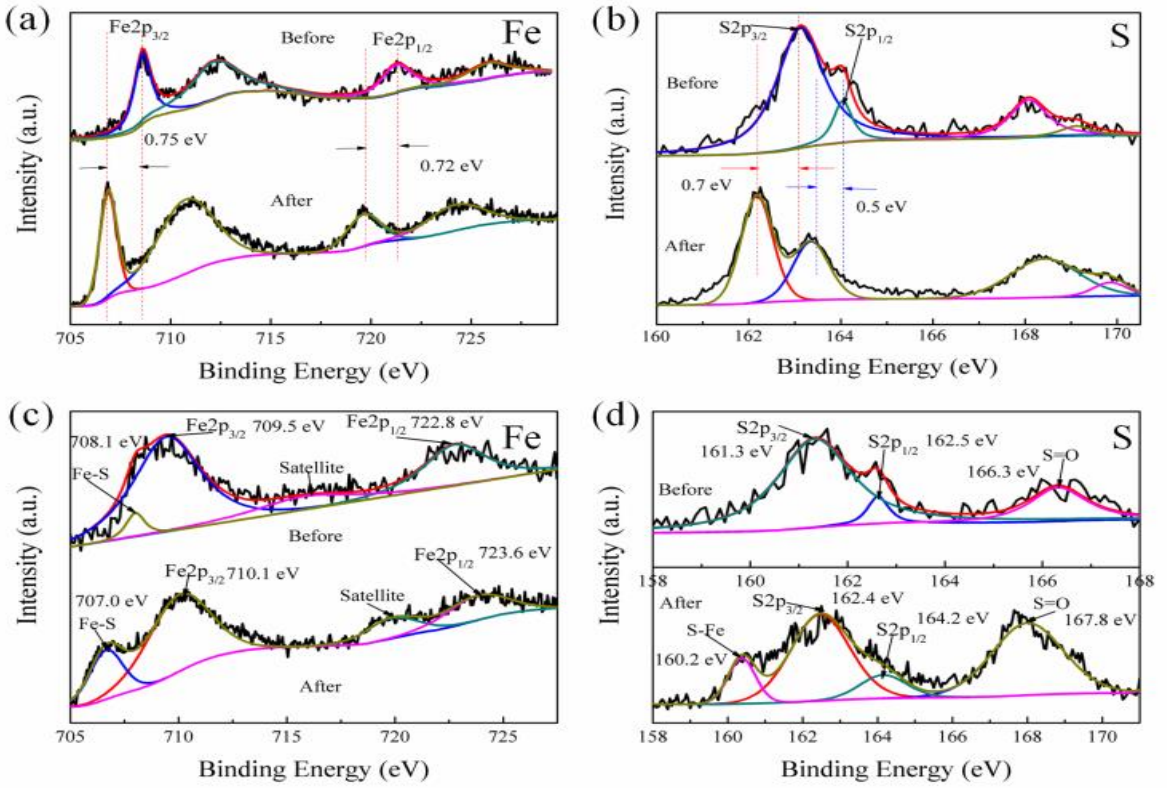

Figure 8. Post catalysis XPS analysis of Fe (a) and S (b) for FeS_2@rGO, Fe (c) and S (d) for FeS@rGO.

It could be found that the collected ring current is much lower than disk current, indicating that the less intermediate product (H_2O_2) and the approximately four-electron transfer pathway for ORR. The Faradaic efficiency was calculated by test of the continuous OER (disk electrode)-ORR (ring electrode) process using the RRDE. The Faradaic efficiency was calculated by the equation followed:

$$\varepsilon = I_r/(I_d * N) \quad (9)$$

Where I_r is the collected ring current of 45 μA, I_d is the disk current, N is the current collection efficiency (0.39 in this study). After calculation, the Faradaic efficiency of FeS, FeS@rGO, FeS_2, and FeS_2@rGO is 73.2%, 83.5%, 77.1% and 87.9%, respectively. Due to the generation of hydrogen peroxide, the Faraday efficiency will be affected by it and will be reduced to some extent. The occurrence of side reactions during the reaction has certain negative effects on the oxygen reduction reaction. For example, hydrogen evolution or the generation of hydrogen peroxide is the cause of the decrease in Faraday efficiency. Faraday's efficiency is one of the criteria for judging material stability. The stability of the material should also be combined with other test results, such as the i-t curve. The Faraday efficiency of FeS2@RGO is the highest among the four catalyst materials, which is also consistent with the measured i-t curve, which proves the stability of the prepared FeS2@RGO material. Figure 8 showed the Post catalysis XPS analysis of FeS_2@rGO and FeS@rGO. It was clearly showed that the binding energy of the Fe and S of FeS_2@rGO and FeS@rGO had a small shift after the reaction, which meant that no chemical bond changes happened during the reaction. The post analysis XPS of the catalyst also proved the long-term running stability of FeS_2@rGO and FeS@rGO. The similar results of FeS_2 and FeS were also obtained the results are showed in the Figure S14. The results of Faradaic Efficiency determination and post catalysis XPS analysis were consistent with the long-time running stability test, which certified the high long-time running stability of the catalysts.

Based on the above results, it can be seen that the hybrid of FeS@rGO and FeS_2@rGO show better catalytic performance for ORR than the pristine FeS and FeS_2. This can be attributed to the synergistic effects between rGO and FeS_2/FeS, which alter the surface electron configuration for oxygen adsorption/activation and provide networks for efficient electron transfer.[36] On the other hand, among all the catalysts, the FeS_2@rGO shows the highest catalytic efficiency and lowest polarization for ORR. The shortened Fe-S bond length of FeS_2 favors the low-spin (S = 0) ground state of electrons compared with the high-spin FeS,[37] which is benefit to the happening of the ORR. Impressively, the peak current intensity and the onset potential of FeS_2@rGO are quite close to that of the super Pt/C catalyst. The long-time running stability of FeS_2@rGO is even better than that of Pt/C catalyst.[38] It could be forecasted that the FeS_2@rGO has great potential to be a high performance substitute for the precious metal-based catalysts for ORR.

Conclusions

In summary, FeS@rGO and FeS_2@rGO catalysts are prepared via a facile method, and their electrocatalytic performances for ORR are reported. Results show that the FeS@rGO and FeS_2@rGO catalysts show much better catalytic activity for ORR than the pristine FeS or FeS_2, which should be attributed to the synergistic effect between rGO and metal sulfides. Remarkably, the onset potentials of FeS_2@rGO catalyzed ORR is close to that of Pt/C catalyst. The long-time running stability of FeS_2@rGO surpasses that of Pt/C catalyst. Based on the research, it can be concluded that the low cost, high performance Fe-based sulphide based catalysts have great potential to be substitute for the precious-based catalysts for ORR. This work provides some new insights for further design of high efficient non-noble metal based electrocatalysts for ORR through constructing novel nano-structured graphene based composites.

Supporting Information Summary

Experimental details including chemical reagents, synthesis procedure of the FeS, FeS@rGO, FeS_2 and FeS_2@rGO, detailed characterisation techniques, electrochemical measurements, materals characterisation data including XPS survey spectra, SEM images, EDS spectrum, and electrochemical measurements of FeS, FeS@rGO, FeS_2 and FeS_2@rGO.

Acknowledgements

This work was financially supported by the Science Development Project of Shandong Province (No. 2017GGX40115, 2016GGX102038) and the National Natural Science Foundation of China (No. 21407060). The authors would like to thank the shiyanjia lab for the supporting of XPS analysis. The authors also would like to thank Dr. Tania Silver at the University of Wollongong for English editing.

Keywords: Catalysis; Electrocatalysts; FeS; FeS_2; Oxygen reduction reaction; Reduced graphene oxide

[1] a) B. C. H. Steele, J. Mater. Sci. **2001**, *35*, 1053-1068; b) K. Ahmed, K. Föger, *Ind. Eng. Chem. Res.* **2010,** *49*, 7239-56; c)X. Zhou, J. Qiao, L. Yang, J. Zhang, J. *Adv. Energy Mater.* **2014**, *4*, 1301523; d) S. C. Singhal, *Solid State Ionics* **2000,** *135*, 305-313; e) Y.J. Wang, J. Qiao, R. Baker, J. Zhang, *Chem. Soc. Rev*. **2013,** *42*, 5768-5787; f) B. C. H. Steele, *Nature* **2001,** *414*, 345-352.

[2] a) L. Gan, Heggen, M. Heggen, O'Malley, R. O'Malley, B. Theobald, P. Strasser, *Nano Lett.* **2013,** *13*, 1131-1138; b) M. S. Çögenli, S. Mukerjee, A. B. Yurtcan, *Fuel Cells* **2015**, *15*, 288-297; c) E. P. Murray, T. Tsai, S. A. Barnett, *Nature* **1999**, *400*, 649; d) F. Cheng, J. Chen, *Chem. Soc. Rev*. **2012,** *41*, 2172-2192.

[3] a) E. Gülzow, *Fuel Cells* **2004,** 4, 251-255; b) G. Merle, M. Wessling, K. Nijmeijer, *J. Membr. Sci*. **2011,** *377*, 1-35.

[4] a) Y. Sun, C. Li, G. Shi, *J. Mater. Chem.* **2012,** *22*, 12810; b) M. Chen, J. Liu, W. Zhou, J. Lin, Z. Shen, *Sci. Rep*. **2015,** *5*, 10389.

[5] a) L. Lai, J. R. Potts, D. Zhan, L. Wang, C. K. Poh, C. Tang, H. Gong, Z. Shen, J. Lin, R. S. Ruoff, *Energ Environ. Sci*. **2012,** *5*, 7936-7942; b) Z.H. Sheng, H.L. Gao, W.-J. Bao, F.B. Wang, X.H. Xia, *J. Mater. Chem*. **2012,** *22*, 390-395; c) K. Gong, F. Du, Z. Xia, M. Durstock, L. Dai, *Science* **2009,** *323*, 760-764.

[6] a) Y. Feng, N. Alonso-Vante, *Phys. status solidi B*. **2008,** *245*, 1792-1806; b) M. S. Faber, M. A. Lukowski, Q. Ding, N. S. Kaiser, S. Jin, *J. Phys. Chem. C* **2014,** *118*, 21347-21356; c) M.R. Gao, J. Jiang, S.H. Yu, *Small* **2012,** *8*, 13-27.

[7] Y. C. Wang, Y. J. Lai, L. Song, Z. Y. Zhou, J. G. Liu, Q. Wang, X. D. Yang, C. Chen, W. Shi, Y.P. Zheng, M. Rauf, S.G. Sun, *Angew. Chem. Int. Ed*. **2015,** *54*, 9907-9910.

[8] F. Rodríguez-Reinoso, *Carbon* **1998,** *36*, 159-175.

[9] J. Lee, J. Kim, T. Hyeon, *Adv. Mater*. **2006,** *18*, 2073-2094.

[10] E. Frackowiak, *Phys. Chem. Chem. Phys*. **2007,** *9*, 1774-85.

[11] M. S. Dresselhaus, P. Avouris, Introduction to carbon materials research. *Vol. 80* (Eds.: M. S. Dresselhaus, G. Dresselhaus, P. Avouris) Springer, Berlin and Heidelberg, **2001**, pp. 1-9.

[12] a) T. Huang, S. Mao, G. Zhou, Z. Wen, X. Huang, S. Ci, J. Chen, *Nanoscale* **2014,** *6*, 9608-9613; b) T. Huang, S. Mao, H. Pu, Z. Wen, X. Huang, S. Ci, J. Chen, *J. Mater. Chem. A* **2013,** *1*, 13404-13410.

[13] a) Y. Hou, T. Huang, Z. Wen, S. Mao, S. Cui, J. Chen, *Adv. Energy. Mater*. **2014,** *4*, 1400337; b) X. Yuan, H.D. Sha, X.L. Ding, H.C. Kong, H. Lin, W. Wen, T. Huang, Z. Guo, Z.F. Ma, Y. Yang, *Int. J. Hydrogen Energy* **2014,** *39*, 15937-15947.

[14] a) M. D. Meganathan, S. Mao, T. Huang, G. Sun, *J. Mater. Chem. A*. **2017,** *5*, 2972-2980; b) J. Xu, P. Gao, T.S. Zhao, Energ. Environ. Sci. **2012**, *5*, 5333-5339; c) F. Cheng, T. Zhang, Y. Zhang, J. Du, X. Han, J. Chen, Angew. Chem. Int. Ed. **2013**, *52*, 2474-2477; d) Y. Zhao, K. Kamiya, K. Hashimoto, S. Nakanishi, *J. Phys. Chem. C* **2015,** *119*, 2583-2588.

[15] S. Kong, Z. Jin, H. Liu, Y. Wang, *J. Phys. Chem. C* **2014**, *118*, 25355-25364.

[16] Jr. Hummers, S. W, R. E. Offeman, *J. Am. Chem. Soc.* **1958**, *80*, 1339-1339.

[17] S. Park, J. An, J. R. Potts, A. Velamakanni, S. Murali, R. S. Ruoff, *Carbon* **2011**, *49*, 3019-3023.

[18] D. Yan, Y. Li, J. Huo, R. Chen, L. Dai, S. Wang, *Adv. Mater*. **2017**,1606459.

[19] a) K. Chang, W. Chen, *ACS Nano* **2011**, *5*, 4720-4728; b) D. Long, W. Li, L. Ling, J. Miyawaki, I. Mochida, S.-H. Yoon, *Langmuir* **2010**, *26*, 16096-16102.

[20] L. Xu, Y. Hu, H. Zhang, H. Jiang, C. Li, *ACS Sustain. Chem. Eng.* **2016,** *4*, 4251-4255.

[21] a) J. Zhang, H. Yang, G. Shen, P. Cheng, J. Zhang, S. Guo, *Chem. Commun*. **2010,** *46*, 1112-1114; b) Y. Li, W. Li, T. Ke, P. Zhang, X. Ren, L. Deng, *Electrochem. Commun*. **2016,** *69*, 68-71.

[22] M. Nath, A. Choudhury, A. Kundu, C. N. R. Rao, *Adv. Mater*. **2003,** *15*, 2098-2101.

[23] J. Liu, L. Wan, M. Zhang, K. Jiang, K. Song, J. Wang, T. Ikeda, L. Jiang, *Adv. Funct. Mater*. **2017**, *27*, 1605221.

[24] M. Shen, C. Ruan, Y. Chen, C. Jiang, K. Ai, L. Lu, *ACS Appl. Mater. Interfaces* **2015,** *7*, 1207-1218.

[25] D. Susac, L. Zhu, M. Teo, A. Sode, K. C. Wong, P. C. Wong, R. R. Parsons, D. Bizzotto, K. A. R. Mitchell, S. A. Campbell, *J. Phys. Chem. C* **2007,** *111*, 18715-18723.

[26] X. Sun, Y. Zhang, P. Song, J. Pan, L. Zhuang, W. Xu, W. Xing, *ACS Catal.* **2013**, *3*, 1726-1729.

[27] Y. Zhu, B. Zhang, X. Liu, D.W. Wang, D. Su, *Angew. Chem*. **2014,** *53*, 10673-10677.

[28] K. N. Kudin, B. Ozbas, H. C. Schniepp, R. K. Prud'Homme, I. Aksay, R. Car, *Nano Lett*. **2008,** *8*, 36-41.

[29] a) J. Liang, Y. Jiao, M. Jaroniec, S. Qiao, *Angew. Chem.* **2012**, *51*, 11496-11500; b) J. Yu, X. Gao, G. Chen, X. Yuan, *Int. J. Hydrogen Energy* **2016,** *41*, 4150-4158.

[30] H. Yang, S. Zhang, L. Han, Z. Zhang, Z. Xue, J. Gao, Y. Li, C. Huang, Y. Yi, H. Liu, Y. Li, *ACS Appl. Mater. Interfaces* **2016**, *8*, 5366-75.

[31] Z. Li, B. Li, Z. Liu, Z. Liu, D. Li, *RSC Adv*. **2015,** *5*, 106245-106251.

[32] a) E. Peled, *J. Electrochem. Soc.* **1979,** *126*, 2047-2051; b) P. Velasquez, D. Leinen, J. Pascual, J. R. Ramos-Barrado, P. Grez, H. Gomez, R. Schrebler, R. Del. Río, R. Cordova, *J. Phys. Chem. B* **2005**, *109*, 4977-4988; c) C. Wen, X. Gao, T. Huang, X. Wu, L. Xu, J. Yu, H. Zhang, Z. Zhang, J. Han, H. Ren, *Int. J. Hydrogen Energy* **2016,** *41*, 11099-11107.

[33] X. Wu, X. Gao, L. Xu, T. Huang, J. Yu, C. Wen, Z. Chen, J. Han, *Int. J. Hydrogen Energy* **2016,** *41*, 16087-16093.

[34] J. Jiang, S. Lu, H. Gao, X. Zhang, H.-Q. Yu, *Nano Energy* **2016,** *27*, 526-534.

[35] W. Ai, Z. Luo, J. Jiang, J. Zhu, Z. Du, Z. Fan, L. Xie, H. Zhang, W. Huang, T. Yu, *Adv. Mater.* **2014**, *26*, 6186-6192.

[36] a) J.M. You, M. S. Ahmed, H. Han, J. e. Choe, Z. Üstündağ, S. Jeon, *J. Power Sources* **2015**, *275*, 73-79; b) N. Ramaswamy, S. Mukerjee, *J. Phys. Chem. C* **2011**, *115*, 18015-18026; c) Y. Zheng, Y. Jiao, J. Chen, J. Liu, J. Liang, A. Du, W. Zhang, Z. Zhu, S. C. Smith, M. Jaroniec, G. Lu, S. Qiao, *J. Am. Chem. Soc.* **201**1, *133*, 20116-20119.

[37] A. Fujimori, K. Mamiya. T. Mizokawa, T. Mayadai, T. Sekiguchi, H. Takahashi, N. Mori. S. Suga. *Phys. Rev. B* **1996**, *54*, 16329.

[38] S. Bag, B. Mondal, A. K. Das, C. R. Raj, *Electrochim Acta* **2015**, *163*, 16-23.

Entry for the Table of Contents

FULL PAPER

FeS@rGO and FeS_2@rGO were synthesized in a simple way. These compounds exhibited outstanding electrocatalysis activity and excellent electrochemical durability for oxygen reduction reaction (ORR) in alkaline media.

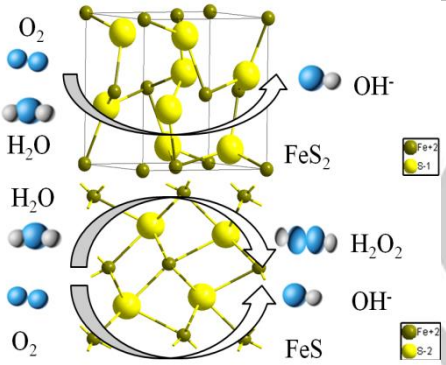

Hengyi Fang,[a] Taizhong Huang,[a] Jianfeng Mao,**[b] Shuo Yao,[a] M. Mayilvel Dinesh,[a] Yue Sun,[a] Dong Liang,[a] Lei Qi,[a] Jiemei Yu[a] and Zhankun Jiang[a]*

Page No. – Page No.

Investigation on the catalytic Performance of Reduced Graphene Oxide Interpolated FeS_2 and FeS for Oxygen Reduction Reaction